



UvA-DARE (Digital Academic Repository)

Modeling the functioning of YtvA in the general stress response in *Bacillus subtilis*

van der Steen, J.B.; Nakasone, Y.; Hendriks, J.C.; Hellingwerf, K.J.

DOI

[10.1039/c3mb70124g](https://doi.org/10.1039/c3mb70124g)

Publication date

2013

Document Version

Final published version

Published in

Molecular BioSystems

[Link to publication](#)

Citation for published version (APA):

van der Steen, J. B., Nakasone, Y., Hendriks, J. C., & Hellingwerf, K. J. (2013). Modeling the functioning of YtvA in the general stress response in *Bacillus subtilis*. *Molecular BioSystems*, 9, 2331-2343. <https://doi.org/10.1039/c3mb70124g>

General rights

It is not permitted to download or to forward/distribute the text or part of it without the consent of the author(s) and/or copyright holder(s), other than for strictly personal, individual use, unless the work is under an open content license (like Creative Commons).

Disclaimer/Complaints regulations

If you believe that digital publication of certain material infringes any of your rights or (privacy) interests, please let the Library know, stating your reasons. In case of a legitimate complaint, the Library will make the material inaccessible and/or remove it from the website. Please Ask the Library: <https://uba.uva.nl/en/contact>, or a letter to: Library of the University of Amsterdam, Secretariat, P.O. Box 19185, 1000 GD Amsterdam, The Netherlands. You will be contacted as soon as possible.

UvA-DARE is a service provided by the library of the University of Amsterdam (<https://dare.uva.nl>)

Modeling the functioning of YtvA in the general stress response in *Bacillus subtilis*[†]

Cite this: *Mol. BioSyst.*, 2013, **9**, 2331

Jeroen B. van der Steen, Yusuke Nakasone,[‡] Johnny Hendriks[§] and Klaas J. Hellingwerf^{*}

The blue-light photoreceptor YtvA activates the general stress response (GSR) of *Bacillus subtilis* by activating a large protein complex (the stressosome). We have constructed a model for the YtvA's photocycle, and derived an equation for the fraction of YtvA in the light-induced signaling state at a given light intensity. The model was verified experimentally *in vitro* on wild type YtvA and on an R63K mutant with faster recovery kinetics. Application of the model to the activation of the GSR at various light intensities *in vivo* revealed that the GSR is more sensitive to light than would be expected based on YtvA's *in vitro* kinetics. These results were confirmed with the R63K mutant and a slower-recovering V28I mutant. Additionally, we have demonstrated the presence of a near-UV-light-induced branching reaction that converts the signaling state of YtvA to the dark state. Extension of the model with this reaction shows that it does not contribute significantly to the *in vivo* blue-light response. The model represents an important step towards a complete systems biology model of the GSR.

Received 28th March 2013,
Accepted 31st May 2013

DOI: 10.1039/c3mb70124g

www.rsc.org/molecularbiosystems

Introduction

Photoreceptor proteins are involved in many important regulatory processes in all kingdoms of life. Several different photoreceptor classes have been identified, of which the input domains can bind a small chromophore such as a flavin, retinal or bilin, allowing these proteins to absorb in the UV/visible region of the electromagnetic spectrum.¹ When they absorb light there are typically significant changes in the absorption spectrum of the photoreceptor protein which can readily be observed with spectroscopic techniques *in vitro*. Hence, a large body of literature is available on the kinetic properties and intermediate species of photoreceptor proteins. However, it is often hard to relate effects of perturbations in their kinetic properties (brought about *e.g.* through site-directed mutagenesis) to *in vivo* phenotypes.

YtvA is a blue-light photoreceptor from the common soil bacterium *Bacillus subtilis*.^{2,3} YtvA has two domains: an N-terminal

LOV (light oxygen voltage) domain and a C-terminal STAS (sulfate transporter and anti-sigma factor antagonist) domain. LOV domains are members of the family of PAS-domains (Per-ARNT-Sim), and were first identified in phototropins found in plants. LOV domains are also found in an increasing number of bacteria.^{4–8} LOV domains bind a flavin mononucleotide (FMN) in a binding pocket with a highly conserved sequence motif. In the case of YtvA this results in a molecule with maximal absorbance at 448 nm in the dark. Illumination with blue light triggers a photocycle (Fig. 1A). After formation of the triplet excited state of FMN through internal conversion on the ns timescale (D^* in Fig. 1A), a thiol adduct is formed between cysteine 62 and the C4a atom of the FMN on the μ s timescale. The resulting signaling state (S), which has an absorbance maximum at 390 nm, thermally converts back to the dark state (D) with a recovery lifetime of 2600 s (at 25 °C).⁹

YtvA is an interesting target for systematic quantitative studies because the full-length protein can readily be purified and its biological function is well-characterized. As a soil organism, *B. subtilis* can respond in multiple ways to fluctuating environmental conditions. One of the most important of these is the general stress response (GSR), which activates 150–200 genes in response to a wide range of stresses.^{10–12} These stresses can be subdivided into two groups: energy stresses (starvation) and environmental stresses (such as NaCl shock, ethanol shock or heat shock). YtvA renders the environmental GSR sensitive to

Molecular Microbial Physiology Group, Swammerdam Institute for Life Sciences and the Netherlands Institute for Systems Biology, University of Amsterdam, P.O. Box 94232, 1090 GE Amsterdam, The Netherlands.

E-mail: K.J.Hellingwerf@UvA.nl; Fax: +31 (0)20 525 7934; Tel: +31 (0)20 525 7055

[†] Electronic supplementary information (ESI) available. See DOI: 10.1039/c3mb70124g

[‡] Current address: Department of Chemistry, Graduate School of Science, Kyoto University, Kyoto, Japan.

[§] Current address: Institute of Complex Systems 4 (ICS-4), Zelluläre Biophysik, Forschungszentrum Jülich GmbH, 52425 Jülich, Germany.

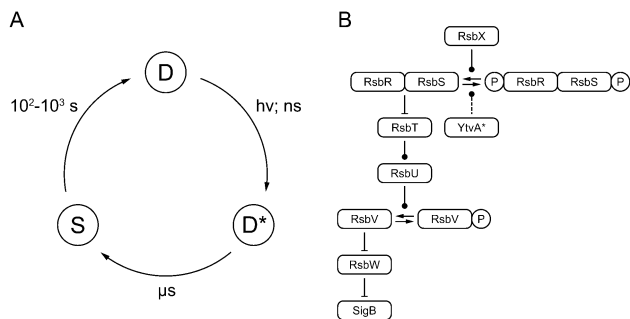


Fig. 1 YtvA's photocycle and biological function (see the text for a comprehensive description). (A) Schematic model of the photocycle of YtvA. (B) The regulatory network of the environmental branch of the general stress response of *Bacillus subtilis*. Arrowheads indicate different types of interactions: arrows with a triangular arrowhead refer to chemical transformations, a flat arrowhead represents inhibition by binding, and a round arrowhead represents activation of a reaction or of a protein. A dashed line indicates an unknown mechanism. A circled 'P' represents a phosphate group. YtvA* indicates that YtvA is in the light-induced signaling state when it activates the stressosome.

blue light. When YtvA is over-expressed, low intensities of blue light result in strong GSR activation.² At wild type expression levels the effects of YtvA are more modest. Nevertheless, GSR activation induced by NaCl-shock is enhanced by light,^{2,13} and a clear transient light-dependent activation of the GSR is seen if a negative regulator of YtvA is knocked out.¹⁴

The signaling network that regulates the environmental GSR is shown in Fig. 1B. A comprehensive description of this network goes beyond the scope of this paper, but extensive reviews have been published elsewhere.¹⁵ Briefly, the activity of the GSR is regulated by the alternative transcription factor SigmaB, which in turn is regulated by a partner-switch consisting of the anti-sigma factor RsbW and the anti-anti-sigma factor RsbV (Rsb: regulator of SigmaB). The activity of the partner switch is controlled through the phosphorylation state of RsbV, which needs to be in the non-phosphorylated form to capture RsbW and release SigmaB. The phosphatase responsible for the environmental GSR is RsbU, which is activated and turns on the GSR when bound to RsbT. To prevent activation in unstressed cells, RsbT is captured by a large protein complex called the stressosome.^{16–18} The stressosome consists of multiple copies of RsbS and of multiple copies of proteins from the RsbR family, which has at least four members.¹⁹ Both RsbS and the RsbR proteins contain a C-terminal STAS domain, as does YtvA. YtvA has been co-purified with other stressosome components²⁰ and has recently been shown to displace RsbRA in stressosomes *in vitro* independently of its illumination state.²¹

We have used YtvA to study the influence of changes in kinetic parameters of a photoreceptor (YtvA) on its biological function (GSR activation), linking microscopic rate constants to biological phenotypes in a systems biology approach. We have constructed a detailed kinetic model of the photocycle of YtvA to model the fraction of protein that is in the light-induced signaling state at a given light intensity. This model was verified using the isolated protein *in vitro*. We have then compared this

to experimentally obtained data for the activation of the GSR, which was determined using a well-characterized and often-employed reporter-enzyme assay.^{2,15,22} The model was further tested with two mutants of YtvA with altered kinetics: R63K, which has a faster recovery of the dark state than the wild type protein,²³ and V28I, which has a slower recovery.²⁴ Additionally, we have demonstrated the presence of a light-induced branching reaction, emerging from the signaling state of YtvA, and examined the possible influence of this branching reaction on the biological activity of YtvA.

Results

Modeling the activation of YtvA

The known reactions and microscopic properties of the photocycle of YtvA (Fig. 1A) were incorporated into a kinetic model, schematically shown in Fig. 2A. In this model, which was based on a previously published general photocycle model for PYP,²⁵ k_{exD} describes the rate of excitation, k_{pe} the rate of photocycle entry, k_{re} the rate of recovery of the dark state, and Q_{yD} the quantum yield of photocycle entry. All parameters, save for k_{exD} , have been determined experimentally *in vitro* (see the legend of Fig. 2 and Table 1). Using these parameters, it is possible to derive differential equations for the concentration of every species (eqn (1)–(3)), which can be used to numerically simulate the temporal dynamics and steady-state levels of the species distribution of YtvA.

For the rate of excitation we assumed that every photon absorbed will first lead to formation of the excited state (D*), after which a certain fraction (the quantum yield of photocycle entry) will continue in the photocycle, while the rest will fall back to the dark state (D) without entry into the photocycle (*e.g.* by fluorescence or heat release). This assumption enables the use of the Lambert–Beer law for absorption, to derive the number of photons absorbed per time unit, from which the k_{exD} reaction rate can be derived (eqn (4); see Materials and methods for details).

$$\frac{d[D]}{dt} = -k_{\text{exD}}[D] + \left(\frac{1}{Q_{\text{yD}}} - 1\right)k_{\text{pe}}[D^*] + k_{\text{re}}[S] \quad (1)$$

$$\frac{d[D^*]}{dt} = k_{\text{exD}}[D] - \frac{k_{\text{pe}}}{Q_{\text{yD}}}[D^*] \quad (2)$$

$$\frac{d[S]}{dt} = k_{\text{pe}}[D^*] - k_{\text{re}}[S] \quad (3)$$

$$k_{\text{exD}} = \frac{I_0(1 - 10^{-\epsilon_D I [D]})}{I[D]} \approx I_0 \epsilon_D \ln(10) \quad (4)$$

In its full form, k_{exD} is dependent on the concentration of the protein in the dark state ($[D]$), the extinction coefficient of the dark state of the protein for the light source used (ϵ_D), the path length (l) and the light intensity (I_0). When the rate equation is approximated using a Taylor expansion, the dependency on $[D]$ can be eliminated (eqn (4)), which allows one to analytically derive fractions for all three protein species in steady state

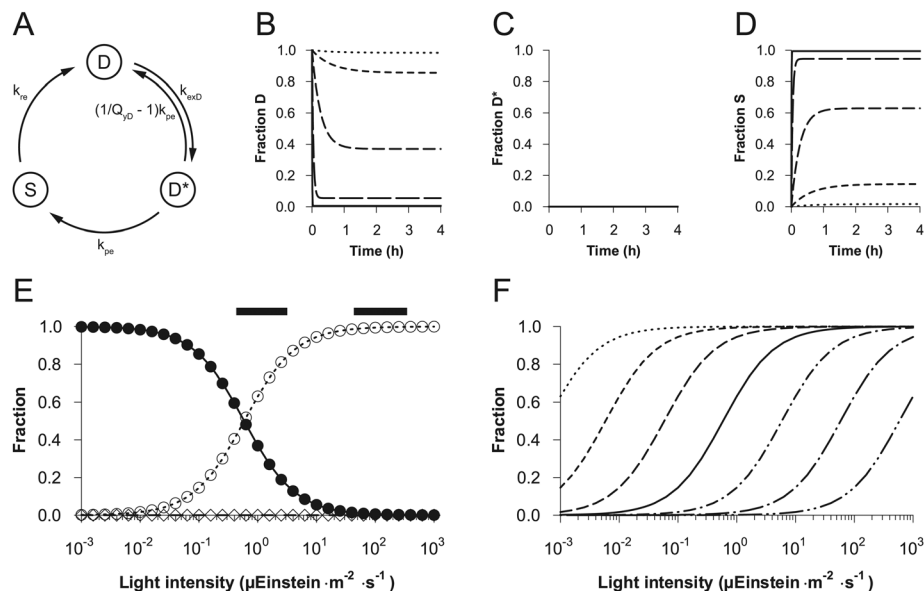


Fig. 2 Quantitative model for the photocycle of YtvA. (A) Representation of the relevant reaction rates and states of YtvA in the model. (B–D) Changes in time of the fraction of the different protein species (D, D* and S, respectively) as simulated using eqn (1)–(3) for various light intensities: 0.01 (dotted lines), 0.1 (square-dotted lines), 1 (short-dashed lines), 10 (long-dashed lines), and 100 (solid lines) $\mu\text{Einstein m}^{-2} \text{s}^{-1}$. Note that the lines in panel C are not visible because there is no significant contribution of D* on this timescale. (E) Distribution of the three species of YtvA in the steady state, using either steady-state eqn (5)–(7) (symbols) or differential eqn (1)–(3) (lines, no symbols). The solid line and filled circles represent the dark state (D), the dotted line and open circles the light-induced signaling state (S), and the open diamonds the excited state (D*); the line corresponding to this species is indistinguishable from the x-axis. The two black bars at the top indicate a crude estimation of relevant laboratory light intensity (the left bar) and daylight intensity (the right bar) in the Netherlands at noon (see Materials and Methods). (F) Effect of changes in the recovery rate on the steady-state fraction of protein in the light-induced signaling state (S). The solid line represents a recovery lifetime ($1/k_{re}$) of 2600 s, the lines to the right lower recovery lifetimes (dot-dash: 260 s, dot-long dash: 26 s and dot-dot-long dash 2.6 s), and the lines to the left higher recovery lifetimes (dashed: 2.6×10^4 s, short-dashed: 2.6×10^5 s and dotted: 2.6×10^6 s). (B–F) The parameters were taken from Losi *et al.*^{3,9} for wild type YtvA *in vitro*: quantum yield (Q_{yD} ; 0.30), photocycle entry rate (k_{pe} ; $5 \times 10^5 \text{ s}^{-1}$) and recovery rate (k_{re} ; $1/2600 \text{ s}^{-1}$ at 25 °C), with the exception of panel F where the recovery rate was varied. Light intensities correspond to illumination with a blue LED ($\lambda_{max} = 464 \text{ nm}$) that was used for experiments (see below).

Table 1 Parameters for the photocycle model

Parameter	Wild type	R63K	R63K	Source
Quantum yield (Q_{yD})	0.30	—	—	3
Photocycle entry rate (k_{pe})	$5 \times 10^5 \text{ s}^{-1}$	—	—	9
Recovery rate (k_{re})	$1.52 \times 10^{-3} \text{ s}^{-1}$	$1.50 \times 10^{-2} \text{ s}^{-1}$	$1.43 \times 10^{-3} \text{ s}^{-1}$	This study
Recovery lifetime ($1/k_{re}$)	658 s	66 s	699 s	This study
Temperature of the experiment	37 °C	37 °C	19 °C	This study

(*i.e.* when eqn (1)–(3) are equal to zero; see Materials and methods for the derivation).

$$f_D = \frac{1}{1 + Q_{yD}k_{exD} \left(\frac{1}{k_{pe}} + \frac{1}{k_{re}} \right)} \quad (5)$$

$$f_{D^*} = \frac{1}{1 + k_{pe} \left(\frac{1}{Q_{yD}k_{exD}} + \frac{1}{k_{re}} \right)} \quad (6)$$

$$f_S = \frac{1}{1 + k_{re} \left(\frac{1}{Q_{yD}k_{exD}} + \frac{1}{k_{pe}} \right)} \quad (7)$$

When eqn (1)–(3) are applied using the parameters for YtvA, determined by Losi *et al.* during their initial *in vitro* characterization of the protein,^{3,9} results such as those shown in

Fig. 2B–D are obtained. In these simulations, all proteins at time point zero are in the dark state. It is then illuminated with different light intensities (the different lines). The results of the simulations match expectations. For example, higher light intensities result in greater accumulation of the light-induced signaling state S. Furthermore, the contribution of the excited state D* to the protein species distribution can be neglected, as expected based on its rapid conversion to the dark state (D) or the light-induced signaling state (S).

Fig. 2E summarizes the results of the numerical simulations by taking only the protein species distribution at equilibrium (lines). The symbols in this figure show the results of the application of the simplified steady-state eqn (5)–(7) to the same parameters. Since both simulations overlap, the validity of the simplification of k_{exD} for a protein with properties like YtvA is confirmed.

One of the advantages of this model is its ability to predict the consequences of changes in parameters. For example,

Fig. 2F shows the predicted influence of changes in the recovery rate on the accumulation of the signaling state at various light intensities. Such predictions are relevant in view of the availability of mutants of YtvA with altered recovery rates (see below).

Application of the model to *in vitro* light titrations

To validate the model, purified YtvA was incubated in a temperature-controlled cuvette at 37 °C under illumination with different light intensities. When a steady state was reached, the fraction of YtvA in the light-induced signaling state (S) was determined from the spectrum of the sample by treating the spectrum as a linear combination of the dark state and the light-induced signaling state (symbols in Fig. 3A).

To simulate the predicted behavior of the protein, the quantum yield and photocycle entry rate were taken from the literature, while the recovery rate was measured in our experimental setup since it strongly depends on temperature (Table 1). The analytical solutions (eqn (5)–(7)) were applied to simulate the predicted fraction of the protein in each of the three states (lines in Fig. 3A). It is clear from the figure that the simulations match the observed values very well without the need for a fit for any of the parameters.

To assess the robustness of the model, a mutant of YtvA with drastically altered recovery kinetics was assayed as well. The R63K mutation was previously shown to accelerate recovery at 20 °C by approximately 8-fold.²³ The mutation was transferred to the same full-length YtvA construct used for the wild type protein, and the process was repeated on purified R63K protein (Fig. 3B). The quantum yield and photocycle entry rate were assumed to be the same as for wild type, and the recovery rate was again determined under the same conditions as the light-intensity titration. As predicted by our model, the very fast recovery kinetics of this mutant did not allow saturation of formation of the light-induced signaling state (S) with our light source at 37 °C (circles in Fig. 3B). Therefore, the temperature was lowered to 19 °C (diamonds in Fig. 3B). The model was able to predict the behavior of the mutant at both temperatures without the need for a fit. Thus, our model gives an accurate

and robust description of the species distribution of YtvA *in vitro*.

Light-intensity dependence of YtvA-mediated GSR activation

Next, we wanted to investigate the behavior of YtvA *in vivo*. YtvA transmits a signal to the stressosome when illuminated by blue light, which in turn activates the general stress response (GSR). We showed previously that there is a correlation between light intensity and the level of GSR activation.²² However, the precise shape of this correlation was not investigated. Using our model, we can now investigate if the fraction of YtvA in the light-induced signaling state correlates with the activation of the GSR.

An established reporter-enzyme assay, based on the genomic insertion of a fusion of the GSR-dependent *ctc* promoter with the gene coding for the β -galactosidase, was used for these experiments. With this system we previously showed the light-dependent activation of the GSR by over-expressed YtvA and by YtvA at wild type expression levels under selected conditions,^{2,14} which was confirmed by microarray analysis.²² Cells were grown in the presence of IPTG to induce over-expression of YtvA. After serial dilutions (see Materials and methods for details) the light was turned on, and a sample was taken after 120 min to ensure that the species distribution of YtvA had enough time to reach a steady state. Dark controls were always included to ensure that there was no light-independent activation of the GSR.

Again, we used both wild type YtvA and the R63K mutant with an approximately 10-fold accelerated recovery rate under our conditions (Table 2). A third mutant, V28I, was included as well. The V28I mutation was previously shown to slow down recovery by approximately 4-fold in the isolated LOV domain of YtvA.²⁴ The mutation was transferred to the full-length construct and its recovery was determined to be approximately 8-fold slower *in vitro* under our experimental conditions (Table 2).

The results (Fig. 4, symbols) resemble the shape of the predictions from our model for all three mutants. Fits of the model with only the recovery rate as a variable—since this parameter is most likely to be influenced by intracellular

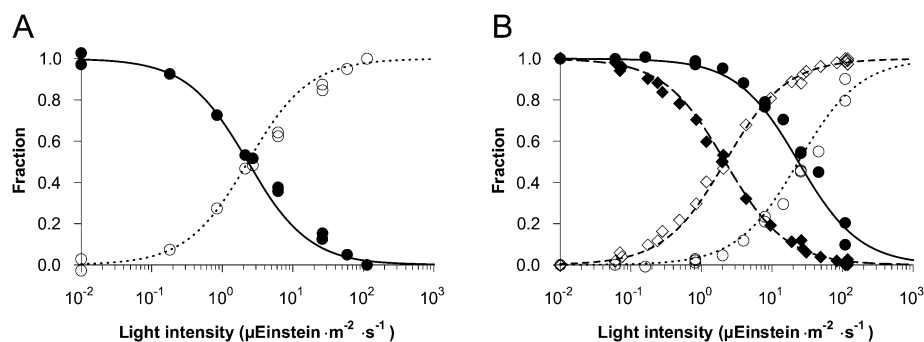


Fig. 3 Fraction of the protein in the light-induced signaling state (S) or in the dark state (D) in steady state when YtvA is illuminated with different light intensities *in vitro*. (A) Wild type YtvA at 37 °C. (B) The R63K mutant at 19 °C (diamonds) and 37 °C (circles). (A–B) Open symbols show the measured fractions of the light-induced signaling state; filled symbols show the measured fractions of the dark state. Dotted and short-dashed lines show simulated fractions of the light-induced signaling state; solid and long-dashed lines simulated fractions of the dark state. Note that, for display purposes, the data obtained without light (i.e. at a light intensity of 0) have been plotted at a light intensity of 0.01 because a logarithmic scale cannot display 0. The data are a composite of multiple measurement series on different days and on different samples.

Table 2 Measured and fitted recovery kinetics of YtvA proteins used in this study (*in vitro* and *in vivo*, respectively) at 37 °C

Mutant	<i>In vitro</i> k_{re}	<i>In vitro</i> $1/k_{re}$	<i>In vivo</i> (fit) k_{re}	<i>In vivo</i> (fit) $1/k_{re}$
Wild type	$1.52 \times 10^{-3} \text{ s}^{-1}$	658 s	$3.47 \times 10^{-4} \text{ s}^{-1}$	2881 s
R63K	$1.50 \times 10^{-2} \text{ s}^{-1}$	66 s	$9.34 \times 10^{-4} \text{ s}^{-1}$	1071 s
V28I	$1.98 \times 10^{-3} \text{ s}^{-1}$	5059 s	$9.61 \times 10^{-5} \text{ s}^{-1}$	10405 s

conditions (see Discussion)—were then simulated (Fig. 4, dashed lines), from which an estimation of the *in vivo* recovery rate was derived (Table 2). Although the values obtained *in vitro* and *in vivo* are quantitatively different, they clearly show a trend: the R63K mutant with faster recovery *in vitro* also requires more light *in vivo* for a maximal activation of the GSR, while the opposite is true for the slower recovering V28I mutant. Thus, the model qualitatively describes the effect of the altered kinetics of YtvA *in vivo*.

The signaling state of YtvA shows a light-induced branching reaction

Above, we have modeled the photocycle of YtvA as a three-step process. However, the light-induced signaling state also absorbs visible light. Many other photoreceptors have photoactive signaling states, leading to processes that are often referred to as ‘branching’ reactions (*e.g.* in PYP,^{26,27} rhodopsins,^{28–31} and phytochromes³²). The presence of such a branching reaction has also been shown for another LOV domain, in which absorption of a near-UV photon results in very fast recovery of the absorption spectrum to the dark state.³³ While Losi and co-workers did not detect a similar reaction during their initial characterization of YtvA, they did state that it may have escaped detection if the yield of this reaction is low.⁹ Therefore, we wondered if the presence of such a reaction could explain the different recovery rates *in vitro* and *in vivo*.

To first prove the existence of the light-induced branching reaction, the light state of YtvA was accumulated by illumination with blue light while its absorption at 450 nm was monitored with low-intensity probe light. The blue lamp was then turned off, resulting in characteristic slow thermal recovery of the dark state (Fig. 5, dotted line). At this point, the sample was

illuminated with a 6 ns flash of 355 nm laser light, a wavelength at which both the dark state and the light state absorb well. Since the dark state was almost fully depleted prior to the laser flash the majority of the light was absorbed by the signaling state. This resulted in very fast recovery of the dark state spectrum in a small fraction of the sample (dashed line), demonstrating the presence of a photo-induced branching reaction. The difference between both signals (solid line) illustrates this fast recovery. Note that the gradual decrease of the relative absorption after induction of the branching reaction can be explained by diffusion of a small amount of YtvA in the light-induced signaling state into the measurement beam.

The quantum yield of this branching reaction was estimated to be 0.2 in the LOV2 domain of phy3 from *Adiantum*.³³ However, its contribution appears to be much lower in YtvA, consistent with the fact that this reaction escaped attention in the original characterization of YtvA.⁹

To make a quantitative estimate of this quantum yield we examined the equilibrium between the dark state and the light-induced signaling state of YtvA under conditions where the thermal recovery can be neglected (*i.e.* at high light intensity and/or at low temperature³³). Under such conditions, the photocycle of

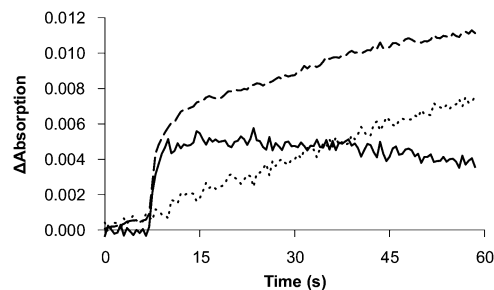


Fig. 5 The signaling state of YtvA displays a light-induced branching reaction. Absorption at 450 nm in time was recorded after accumulation of the signaling state (S) by prolonged illumination with blue light (464 nm). The blue light was switched off at time zero, after which the light-induced branching reaction was induced with a short (6 ns) laser pulse of 355 nm after 7 s. The dotted line displays thermal recovery of the dark state without the laser-induced branching reaction, the dashed line the recovery with laser-induction of the branching reaction, and the solid line shows the difference between both traces.

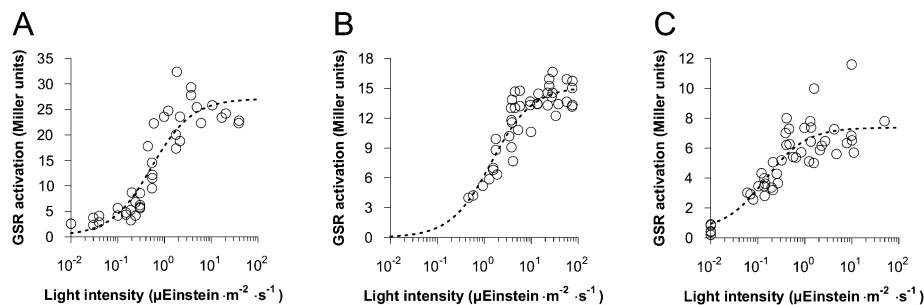


Fig. 4 Light-intensity dependence of GSR activation with wild type YtvA and two site-directed mutants (open circles), and fits with the photocycle model with only the recovery rate as free variable (dashed lines). YtvA was over-expressed prior to the experiment in all strains (see text). Note that, for display purposes, the data obtained without light (*i.e.* at a light intensity of 0) have been plotted at a light intensity of 0.01 because a logarithmic scale cannot display 0. (A) Wild type YtvA. (B) The R63K mutant. (C) The V28I mutant.

YtvA is purely driven by the light source, with the conversion of the dark state to the light-induced signaling state competing with the back-conversion to the dark state. In equilibrium, both rates must be equal so that eqn (8) must hold, in which N_D and N_S represent the number of photons absorbed by the dark state and the light-induced signaling state, respectively. From this, one can derive eqn (9) which yields the quantum yield of the light-induced branching reaction (Q_{YS}). Note that the ratio of the population of the dark state and the light-induced signaling state can easily be determined from the UV/Vis absorption spectrum in equilibrium at saturating light intensities, and that the ratio between absorbed photons is equal to the ratio of spectral overlap between the two states and the actinic light.

$$[S] \times N_S \times Q_{YS} = [D] \times N_D \times Q_{yD} \quad (8)$$

$$Q_{YS} = \frac{[D]}{[S]} \times \frac{N_D}{N_S} \times Q_{yD} \quad (9)$$

To estimate the quantum yield of the light-induced branching reaction we used a light source centered at 401 nm for which the ratio N_D/N_S is equal to 0.92, indicating that both species absorb its light almost equally well. YtvA was illuminated with saturating light intensities, from which a $[D]/[S]$ of ~ 0.06 was derived. Together with the known value for Q_{yD} (0.3) we used eqn (9) to estimate the value of Q_{YS} to be 0.02.

The light-induced branching reaction of YtvA does not significantly contribute to its *in vivo* function

It is straightforward to extend our photocycle model with the light-induced branching reaction. As shown in Fig. 6A three additional reactions and parameters have to be included, with k_{exS} as the rate of excitation of S (similar to k_{exD}), Q_{YS} as the quantum yield of the branching reaction and k_{be} as the rate of branching entry. These additional reactions complicate the differential equations (eqn (10)–(13)). Using the same assumption

for k_{exD} and k_{exS} as made previously, they can nevertheless be solved into equations for the steady-state fractions of the different species of YtvA (eqn (14)–(16)).

$$\frac{d[D]}{dt} = -k_{exD}[D] + \left(\frac{1}{Q_{yD}} - 1\right)k_{pe}[D^*] + k_{re}[S] + k_{be}[S^*] \quad (10)$$

$$\frac{d[D^*]}{dt} = k_{exD}[D] - \frac{k_{pe}}{Q_{yD}}[D^*] \quad (11)$$

$$\frac{d[S]}{dt} = k_{pe}[D^*] - (k_{re} + k_{exS})[S] + \left(\frac{1}{Q_{YS}} - 1\right)k_{be}[S^*] \quad (12)$$

$$\frac{d[S^*]}{dt} = k_{exS}[S] - \frac{k_{be}}{Q_{YS}}[S^*] \quad (13)$$

$$f_D = \frac{1}{1 + k_{exD}Q_{yD} \left(\frac{1}{k_{pe}} + \frac{k_{be} + k_{exS}Q_{YS}}{k_{be}(k_{re} + k_{exS}Q_{YS})} \right)} \quad (14)$$

$$f_{D^*} = \frac{1}{1 + k_{pe} \left(\frac{1}{k_{exD}Q_{yD}} + \frac{k_{be} + k_{exS}Q_{YS}}{k_{be}(k_{re} + k_{exS}Q_{YS})} \right)} \quad (15)$$

$$f_S = \frac{1}{1 + (k_{re} + k_{exS}Q_{YS}) \left(\frac{1}{k_{exD}Q_{yD}} + \frac{1}{k_{pe}} \right) + \frac{k_{exS}Q_{YS}}{k_{be}}} \quad (16)$$

$$f_{S^*} = \frac{1}{1 + \frac{k_{be}}{k_{exS}Q_{YS}} \left(\frac{k_{re} + k_{exS}Q_{YS}}{k_{exD}Q_{yD}} + \frac{k_{re} + k_{exS}Q_{YS}}{k_{pe}} + 1 \right)} \quad (17)$$

To simulate the influence of the branching reaction on the proteins' species distribution the model was applied using the same parameters as in Fig. 2F. The value of k_{be} was taken to be equal to k_{pe} —the laser flash experiment revealed very fast kinetics and faster kinetics do not influence the outcome significantly (data not shown). The quantum yield (Q_{YS}) was taken to be 0.02 (see above). The simulation shows an effect at high light intensities that effectively lowers the fraction of the light-induced signaling state (S) that can be accumulated (Fig. 6B). However, the effect is so small that application of this branching model to the *in vivo* light titration data (Fig. 4) results in less than 1% change of the fitted recovery rate for all three mutants (data not shown).

Discussion

Construction of a model for the photocycle of YtvA

We have constructed a mathematical model for the photocycle of the blue-light photoreceptor YtvA based on its known properties and kinetics. Differential equations were used to simulate the temporal changes in protein species distribution during illumination (eqn (1)–(3); Fig. 2). From this model we analytically derived equations for the fraction of the protein in each species in steady state (eqn (5)–(7)). These equations were applied to light-intensity titration experiments *in vitro* to

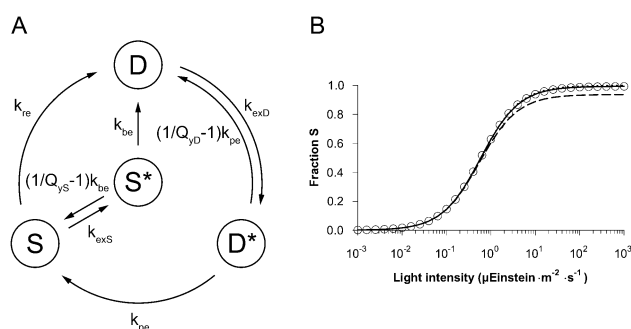


Fig. 6 Model for the photocycle of YtvA that includes the light-induced branching reaction. (A) Schematic representation of the model. (B) Fraction of YtvA in the light-induced signaling state S at varying light intensities and quantum yields of branching (Q_{YS}). Parameters are the same as in Fig. 2E, with as added parameters the branching entry rate (k_{be} ; $5 \times 10^5 \text{ s}^{-1}$) and quantum yield of the branching reaction. Lines represent the steady-state solutions of the differential equations of the model; open circles represent the solutions of the simplified steady-state equations. Solid line and open circles: a Q_{YS} of 0.02 (as determined here for YtvA); dotted line: simple model without branching (effectively Q_{YS} of 0); dashed line: Q_{YS} of 0.2 (as for *Adiantum* LOV2). Note that the dotted line and the solid line overlap.

validate the assumptions made in the model. The model predicted the behavior of wild type YtvA *in vitro* extremely well without a need for fitting, which was also true for a mutant with altered recovery kinetics (Fig. 3).

It is interesting to note that the steady-state equations for the dark state and the signaling state (eqn (1) and (3)) can be simplified to eqn (28) and (29). Also, when some reasonable assumptions are made, a simple analytical expression can be derived to approximate the temporal changes in protein species distribution when light conditions change (eqn (30)). From there another expression can be derived to determine the time it takes to reach a certain percentage of a new steady-state value after a change in light conditions (eqn (31)). Together, these equations form a toolkit for the prediction of required conditions for a given experiment that involves a photoreceptor (see Materials and methods and ESI† for the derivation and notes on usage).

Application of the model to *in vivo* data

YtvA has the added advantage of having a well-resolved biological role in inducing the general stress response (GSR) of *B. subtilis*. This enabled us to indirectly measure the activation of YtvA through a reporter-enzyme. The results (Fig. 4) closely resemble the shape the model predicts. Most variation likely derives from biological variation and inaccuracy in the determination of the average light intensity in a shaking Erlenmeyer flask. The data show a clear correlation with *in vitro* data: the strain with the faster-recovering R63K mutant of YtvA is less sensitive to light than wild type, while the strain with the slower-recovering V28I mutant is more sensitive instead.

Intriguingly, the sensitivity of the *in vivo* response to light is quantitatively different from the sensitivity of YtvA itself to light. The results of the fits suggest slower recovery kinetics *in vivo* than *in vitro*. As a result, the GSR is more light-sensitive than would be predicted based on the *in vitro* kinetics of YtvA (Table 2). This is exciting, because it suggests that the signal transduction network of the GSR may be highly optimized to increase its sensitivity to harmful high-energy light, while still maintaining a reasonable time resolution. A rationale for this may be the relatively modest molar extinction coefficient of oxidized flavins ($\sim 1.25 \times 10^4 \text{ M}^{-1} \text{ cm}^{-1}$ at the absorption maximum) compared to other photoreceptors that mostly have a several fold higher extinction coefficient.^{34–36}

We cannot derive the *in vivo* feature responsible for this effect from our data because our model does not include all reactions of the signaling pathway. One of the possibilities is that the response to blue light is a cooperative response, as suggested for other environmental stresses that are signaled through the stressosome.³⁷ Alternatively, the curve may be shifted, or its shape may be altered, by the involvement of signal-amplification and feedback loops such as the induction of expression of SigmaB (and its primary regulators RsbV and RsbW) upon stress, the induction of RsbX (a negative regulator of the environmental GSR) or the stressosome component RsbRD.^{12,14,38} A third possibility is involvement of stress-induced degradation of the reporter enzyme (LacZ), as was

recently suggested based on an artificial system,³⁹ which may also alter the shape of the curve. Finally, the environment of YtvA in the cell may not be well-represented by *in vitro* buffer conditions. In general, buffers do not necessarily resemble *in vivo* conditions.^{40–42} However, we observed variations in the recovery rate of less than 10% *in vitro* when the salt concentration was increased up to 300 mM (enough for a GSR stress *in vivo*) or when the pH was varied between 7 and 10 (data not shown), suggesting that YtvA is relatively insensitive to buffer conditions. Still, YtvA is proposed to be a part of the stressosome *in vivo*, which may significantly alter its local environment and consequently its microscopic rate constants, e.g. by stabilization of the light-induced state.

Our results also imply that most experiments on the GSR in *B. subtilis* for which the light climate was not specified, presumably had a significant fraction of YtvA in the light-activated signaling state (Fig. 2E). Thus, this work emphasizes the need to define the light climate in future experiments—even if those experiments do not directly deal with light. The basic eqn (28)–(31) are intended to help with the definition of the optimal experimental light climate.

YtvA has a light-induced branching reaction that does not significantly impair its function

Previously, YtvA was not thought to have a light-induced branching reaction such as found in the LOV2 domain of *phy3* of *Adiantum*.^{9,33} Our data clearly show the presence of such a reaction (Fig. 5), although its quantum yield is low (approximately 0.02).

An extension to our model shows that the effect of this branching reaction *in vivo*, when YtvA is illuminated with a blue LED such as in our experiments, can be neglected (Fig. 6). However, it is worthwhile to note that illumination of YtvA with a light source closer to the UV is predicted to have larger effects. Thus, UV light may have a significant effect on the biological function of YtvA. Additionally, our model predicts that the function of LOV domains such as LOV2 of *phy3* of *Adiantum*, which was reported to have a quantum yield of the branching reaction of 0.2,³³ would be significantly affected (Fig. 6, dashed line).

Future directions for GSR research

We consider YtvA the ideal tool for the study of the GSR in *B. subtilis* because it is the only stress signal which can easily, rapidly and reversibly be controlled. The construction of a model for its photocycle is a significant step towards a kinetic model of the entire signal transduction pathway that regulates the GSR. At present, this is not feasible because there are still too many unknown factors, including the nature and strength of other input signal(s) of the stressosome. Nevertheless, progress has been made with computational models of the RsbV-RsbW-SigmaB partner switch module and the energy stress response,^{43,44} and it will be interesting to combine these two approaches to generate a full systems biology model. Ultimately, such quantitative models for the GSR may contribute to a better understanding of the process of

signal integration, as much as—and complementary to—the chemotaxis system.^{45,46}

Conclusion

Our model is constructed such that it is applicable to every photoreceptor which can be described with a three-state cyclic model. However, the ease of extension of the model with the light-induced branching reaction also shows that the model can easily be modified to accommodate photoreceptors with more complicated photodynamics. This means that the model will be useful *e.g.* for estimation of the light intensity required to achieve a desired effect (given a photoreceptor with known characteristics), and estimation of key kinetics based on preliminary experiments. Additionally, the model will be useful to estimate which parameter can be most effectively changed to achieve a desired effect, which will be useful for *e.g.* application in optogenetics.

Materials and methods

Derivation of the photocycle model

The model for the photocycle of YtvA was based on the approach outlined in Hendriks and Hellingwerf (2009)²⁵ for PYP, with modifications where required. Our model is schematically shown in Fig. 2A. The parameters are: k_{exD} , the rate of excitation; k_{pe} , the rate of photocycle entry; k_{re} , the rate of recovery of the dark state; and Q_{yD} , the quantum yield of photocycle entry. Using this, it is possible to derive differential equations for every species (eqn (1)–(3)), which can be used to numerically simulate the species distribution of YtvA.

The model is based on the assumption that every absorbed photon leads to the formation of the excited state (D^*), which then continues into the photocycle to an extent depending on the quantum yield.²⁵ This allows the application of the Lambert–Beer law for absorption (eqn (18) and (19)) with A the absorption, I_0 and I the light intensities before and after absorption by the sample, ε_{D} the molar extinction coefficient of the protein, l the path length and $[D]$ the concentration of the dark state of the protein.

$$A = \log \frac{I_0}{I} = \varepsilon_{\text{D}} l [D] \quad (18)$$

$$I = I_0 \times 10^{-\varepsilon_{\text{D}} l [D]} \quad (19)$$

The number of photons absorbed is equal to the difference between the light intensity before and after the sample. This light intensity can most easily be expressed in mEinstein $\text{cm}^{-2} \text{s}^{-1}$ ($10^7 \mu\text{Einstein m}^{-2} \text{s}^{-1}$). Thus, to obtain the rate of formation of D^* (ν_{D^*}), the light intensity can be multiplied by the illuminated area (a). Dividing this by the volume of the sample (al) gives the rate of formation of D^* in M s^{-1} (eqn (20)).

$$\nu_{\text{D}^*} = a \frac{I_0 - I}{al} = \frac{I_0 - I}{l} = \frac{I_0(1 - 10^{-\varepsilon_{\text{D}} l [D]})}{l} \quad (20)$$

Taking into account that the rate of formation of D^* is equal to $k_{\text{exD}}[D]$, this results in eqn (21) for k_{exD} . The dependence of

k_{exD} on $[D]$ makes it impossible to obtain analytical solutions for the fraction of protein in any of the three states at steady state. Thus, k_{exD} was approximated by converting the power 10 part of this equation to an exponent (eqn (21)), after which a Taylor expansion for an exponential function (eqn (22)) was used to obtain eqn (23).

$$k_{\text{exD}} = \frac{I_0(1 - 10^{-\varepsilon_{\text{D}} l [D]})}{l [D]} = \frac{I_0(1 - e^{-\varepsilon_{\text{D}} l [D] \ln 10})}{l [D]} \quad (21)$$

$$e^x = \sum_{n=0}^{\infty} \frac{x^n}{n!} = 1 + x + \frac{x^2}{2!} + \frac{x^3}{3!} + \frac{x^4}{4!} + \dots \quad (22)$$

$$k_{\text{exD}} \approx \frac{I_0(1 - (1 - \varepsilon_{\text{D}} l [D] \ln 10))}{l [D]} = I_0 \varepsilon_{\text{D}} \ln 10 \quad (23)$$

In this equation, the molar extinction coefficient (ε_{D}) has to be calculated for the entire spectrum of the light source (see below).

With the dependency of k_{exD} on $[D]$ removed, it is possible to derive equations for the steady-state fraction of YtvA in any of the three states (when eqn (1)–(3) are zero). For example, setting eqn (3) to zero, results in eqn (24). Similarly, setting eqn (2) to zero results in eqn (25), and setting eqn (1) to zero and expressing $[D^*]$ in $[S]$ *via* eqn (24) therein leads to eqn (26).

$$\frac{d[S]}{dt} = k_{\text{pe}}[D^*] - k_{\text{re}}[S] = 0 \quad (24)$$

$$k_{\text{pe}}[D^*] = k_{\text{re}}[S]$$

$$[D^*] = \frac{k_{\text{re}}}{k_{\text{pe}}}[S]$$

$$[D] = \frac{k_{\text{pe}}}{Q_{\text{yD}} k_{\text{exD}}}[D^*] \quad (25)$$

$$[S] = \frac{Q_{\text{yD}} k_{\text{exD}}}{k_{\text{re}}}[D] \quad (26)$$

The fraction in any of the three states is given by the concentration in that state divided by the total concentration, as in eqn (27) for the dark state (D).

$$f_{\text{D}} = \frac{[D]}{[D] + [D^*] + [S]} \quad (27)$$

Expressing concentrations $[D^*]$ and $[S]$ in $[D]$ using eqn (25) and (26) allows one to divide out the concentration $[D]$, which simplifies to eqn (5). A similar approach leads to eqn (6) and (7).

Simulations of steady-state fractions of each of the YtvA species, as well as of time traces based on the differential equations (such as in Fig. 2), were done using Matlab R2010b (MathWorks).

Eqn (5) and (7) can be further simplified by noting that the term $1/k_{\text{pe}}$ is in general much smaller than the term next to it ($1/k_{\text{re}}$ in eqn (5) and $1/(Q_{\text{yD}} k_{\text{exD}})$ in eqn (7)), and can therefore

be neglected. Reorganizing the resulting equations results in eqn (28) and (29).

$$f_D = \frac{1}{1 + Q_{yD}k_{exD} \left(\frac{1}{k_{pe}} + \frac{1}{k_{re}} \right)} \approx \frac{k_{re}}{Q_{yD}k_{exD} + k_{re}} \quad (28)$$

$$f_S = \frac{1}{1 + k_{re} \left(\frac{1}{Q_{yD}k_{exD}} + \frac{1}{k_{pe}} \right)} \approx \frac{Q_{yD}k_{exD}}{Q_{yD}k_{exD} + k_{re}} \quad (29)$$

As the contribution of $[D^*]$ is negligible (see Fig. 2C), one can make the approximation that the total amount of protein is equal to $[D] + [S]$. In addition, it is reasonable to assume that the change in $[D]$ mirrors the change in $[S]$ ($d[D]/dt = -d[S]/dt$). Using these approximations it is possible to derive a simple analytical expression for the temporal changes in protein species distribution for a specific light condition (eqn (30)).²⁵ From this, an expression can be derived for the time it takes to reach a certain percentage of the new steady-state value after a change in light conditions (eqn (31)). In eqn (30), c_{tot} represents the total concentration of protein and $[D]_0$ the concentration of the dark state at time zero. In eqn (31), t represents the time (in seconds) until f_D (the fraction of protein in the dark state) has reached a fraction of $f_{steady\ state}$ of the steady-state value of f_D . For example, if $f_{steady\ state}$ is 0.95, t represents the time it takes for 95% of the change in f_D due to the new light intensity to have taken place.

$$f_D = \left(\frac{[D]_0}{c_{tot}} - \frac{k_{re}}{Q_{yD}k_{exD} + k_{re}} \right) e^{-(Q_{yD}k_{exD} + k_{re})t} + \frac{k_{re}}{Q_{yD}k_{exD} + k_{re}} \quad (30)$$

$$t = \frac{\ln(1 - f_{steady\ state})}{-(Q_{yD}k_{exD} + k_{re})} \quad (31)$$

For a detailed derivation and notes on how to use these equations, see the ESI.† Note that these simplified equations were not used for the simulations shown in the manuscript.

Extension of the photocycle model to include a light-induced branching reaction

The addition of a light-induced branching reaction to our model extends it with three additional reactions (Fig. 6A). Compared to the full basic model outlined above, the extra parameters are: k_{exS} , the rate of excitation of S; Q_{yS} , quantum yield of the branching reaction; and k_{be} , the rate of branching entry. Similar to before, this can be used to set up differential equations to describe the temporal dynamics of each protein species involved (eqn (10)–(13)).

In this model, the form of k_{exS} is equal to k_{exD} , with the exception that now the molar extinction coefficient of the light-induced signaling state (ϵ_S) is used (see below for the calculation). In steady state, when eqn (10)–(13) are zero, it is again possible to express the concentrations of the protein species in each other, resulting in equations for the steady-state fractions (eqn (14)–(17)). For example, the steady-state fraction of the

light-induced signaling state S can be derived by expressing S^* in S through eqn (13), resulting in eqn (32). Substituting this result in eqn (12) allows the expression of D^* in S (eqn (33)), and substituting both results in eqn (10) allows the expression of D in S (eqn (34)). These three equations can then be combined to derive the fraction of the protein that is in state S in steady state (eqn (16)).

$$[S^*] = \frac{k_{exS}Q_{yS}}{k_{be}}[S] \quad (32)$$

$$[D^*] = \frac{k_{re} + k_{exS}Q_{yS}}{k_{pe}}[S] \quad (33)$$

$$[D] = \frac{k_{re} + k_{exS}Q_{yS}}{k_{exD}Q_{yD}}[S] \quad (34)$$

A similar approach can be used to derive the other steady-state fractions (eqn (14)–(17)).

Determination of the effective extinction coefficient of YtvA for a given light source

The rates of excitation for the dark state (k_{exD}) and the light-induced signaling state (k_{exS} , in the branching model) depend on the extinction coefficient for the respective protein species (ϵ) and the light intensity used (I_0). However, as is often the case, the light source used emits a peak over a range of wavelengths for which the extinction coefficient is not constant. Thus, both ϵ and I_0 are functions of the wavelength (λ), and the expression should be an integral over $\epsilon(\lambda)I_0(\lambda)$.

The wavelength-dependent extinction coefficient for the dark spectrum was determined by normalizing the absorption spectrum to $\epsilon_{450} = 12\,500\text{ M}^{-1}\text{ cm}^{-1}$: the extinction coefficient of FMN that was also used for the quantum yield determination by ref. 3. An isosbestic point was used to normalize the light-induced spectrum to the dark spectrum to obtain $\epsilon(\lambda)$ for this species.

The emission spectrum of the blue LED with a λ_{max} of 464 nm that was used for all experiments was determined using an Ocean Optics USB4000 spectrophotometer. Because the total light intensity over all emitted wavelengths ($I_0(\text{total})$) was measured experimentally, $I_0(\lambda)$ was split into two factors: $I_0(\text{total})f(\lambda)$, where $f(\lambda)$ represents the fractional contribution of wavelength λ to the total intensity. In effect $f(\lambda)$ is the emission spectrum of the light source normalized to a total area of 1. The area of overlap between $\epsilon(\lambda)$ and $f(\lambda)$ was used as the 'effective molar extinction coefficient', resulting in $\epsilon_D = 9516\text{ M}^{-1}\text{ cm}^{-1}$ and $\epsilon_S = 963\text{ M}^{-1}\text{ cm}^{-1}$ for the light source used in these experiments.

The two black bars that denote a crude estimate of relevant light intensities in the lab and of sunlight in the Netherlands at noon in Fig. 2E were included for comparative purposes. The light intensity of the lighting in our lab was estimated using a LI-COR LI-250 light meter and a LI-COR Quantum Sensor, and its spectrum was measured using an Ocean Optics USB4000 spectrophotometer. The measured light intensity was then corrected to represent a light intensity with comparable activity

with regard to YtvA activation as the blue LED for which the data in the figure was simulated. Similarly, the solar light intensities were estimated based on the average solar irradiance at noon in De Bilt, the Netherlands in December (lower limit) and June (upper limit),⁴⁷ combined with the solar irradiation spectrum from ASTM Standard G173-03 (global tilted) reproduced with SMARTS v2.9.2.⁴⁸

Plasmid and strain constructions

Strains, plasmids and primers used in this study are listed in Table 3. DNA manipulations and other molecular genetic techniques were carried out using standard procedures. The sequences of all constructed plasmids were verified.

Plasmids suitable for expression and isolation of YtvA mutants were constructed using *E. coli* XL1-Blue as cloning host. *E. coli* M15/pREP4 was then transformed with the constructed plasmids to create production strains. The ytvA(R63K) mutation was amplified using primers pQE30ytvAFW and pQE30ytvARV from a template plasmid carrying the mutation (a kind gift of Wolfgang Gärtner). The PCR product was then digested with BamHI and SalI and ligated into similarly digested pQE-30 to create pYN006. The ytvA(V28I) mutation was constructed using the QuickChange method. Template pQE-30-ytvA was amplified using primers JBS190 and JBS191 to create plasmid pJA024.

Plasmids suitable for expression of YtvA in *B. subtilis* were also constructed using *E. coli* XL1-Blue as cloning host. *E. coli* MC1061, a strain that creates plasmid multimers, was subsequently transformed with the constructed plasmids. The ytvA gene carrying the R63K mutation was amplified from pYN006

with primers OB1 and OB2, digested with SalI and SphI, and ligated into similarly digested pDG148 to create pYN012. The ytvA(V28I) mutation was constructed in a two-step PCR procedure. First, overlapping fragments of the mutated gene were amplified using primers OB1 and JBS191 and JBS190 and OB2. Second, both fragments were used as a template in a PCR with flanking primers OB1 and OB2. The fragment was digested with SalI and SphI and ligated into similarly digested pDG148 to generate pJBS1140 (V28I).

B. subtilis strain PB565,¹⁹ a derivative of the wild-type PB2,⁴⁹ contains a ytvA null mutation and an integration in a neutral site (the amyE gene) of a fusion between the SigmaB-dependent ctc promoter and the lacZ reporter gene (which encodes for a β -galactosidase). This strain was transformed with pYtvA, pYN012 or pJBS1140, isolated from *E. coli* MC1061, to generate the strains used for GSR activation assays.

Protein isolation

E. coli M15/pREP4 with the appropriate plasmid (pQE-30-ytvA for wild type YtvA, pYN006 for the R63K mutant or pJA024 for the V28I mutant) was grown overnight in 20 ml of Production Broth (PB: 20 g l⁻¹ Bacto-trypton, 10 g l⁻¹ yeast extract, 5 g l⁻¹ NaCl, 8.7 g l⁻¹ K₂HPO₄ and 5 g l⁻¹ glucose) supplemented with 50 μ g ml⁻¹ kanamycin and 100 μ g ml⁻¹ ampicillin. The next day, 1 l of PB was inoculated with the overnight culture and grown at 37 °C, with shaking at 250 rpm. When an optical density (OD) at 600 nm of 0.4–0.6 was reached, 1 mM (final concentration) of IPTG was added to induce expression, and the culture was allowed to grow overnight at room temperature. Cell-free extracts were prepared by sonication in buffer A

Table 3 Strains, plasmids and primers_Ref323805782 used in this study

Strain, plasmid or primer	Genotype, characteristic or sequence ^a	Ref.
<i>Bacillus subtilis</i> strains		
PB565	ytvA::ery amyE::(P _{ctc} -lacZ cat) trpC2	19
<i>Escherichia coli</i> strains		
M15/pREP4	Production host	QIAGEN
MC1061	Cloning host	53
XL1-Blue	Cloning host	Stratagene
Plasmids		
pDG148	P _{spac} ::MCS bla kan	54
pJA024	P _{T5} ::ytvA(V28I) bla	This study
pJBS1140	P _{spac} ::ytvA(V28I) bla kan	This study
pYN006	P _{T5} ::ytvA(R63K) bla	This study
pYN012	P _{spac} ::ytvA(R63K) bla kan	This study
pYtvA	P _{spac} ::ytvA bla kan	2
pQE-30	P _{T5} ::MCS bla	QIAGEN
pQE-30-ytvA	P _{T5} ::ytvA bla	55
pR63K	ytvA(R63K)	23
Primers		
JBS190	CGGTGTGATTATTACAGATC	This study
JBS191	GATCTGTAATAATCACACCG	This study
OB1	CCCCGTCGACAAGGAGGAAGCAGGTATGGCTAGTTTT	This study
OB2	CCCGCATGCTTACATAATCGGAAGCACTTTAACG	This study
pQE30ytvAFW	CCCGGATCCATGGCTAGTTTTCAATCATTTGGG	55
pQE30ytvARV	GGGGTCGACTTACATAATCGGAAGCACTTTAACG	55

^a Resistance cassettes: bla for ampicillin resistance, cat for chloramphenicol resistance, ery for erythromycin resistance, and kan for kanamycin resistance. MCS: multiple cloning site. In primer sequences, restriction sites are underlined while altered bases for mutagenesis are in bold.

(20 mM Tris-HCl, 500 mM NaCl, 20 mM imidazole, pH 8.0) supplemented with cOmplete EDTA-free protease inhibitor cocktail (Roche), DNase, RNase and lysozyme.

Poly-histidine-tagged protein was purified using a HisTrap HP 5 ml column (GE Healthcare) and an ÄKTA FPLC system (GE Healthcare) using a linear gradient from 20 to 500 mM imidazole in 20 mM Tris-HCl, 500 mM NaCl, pH 8.0. Fractions containing the protein were collected and dialyzed against 20 mM Tris-HCl pH 8.0. The protein was then further purified on a 6 ml Resource Q column (GE Healthcare) using a linear gradient from 0 to 1 M NaCl in 20 mM Tris-HCl pH 8.0. Again, fractions containing the protein were dialyzed against 20 mM Tris-HCl, 10 mM NaCl, pH 8.0. Protein purity was checked *via* SDS-PAGE.

***In vitro* photocycle measurements and data analysis**

All *in vitro* photocycle measurements were done with an Agilent 8453 UV-Vis spectrophotometer (Agilent Technologies) using a Kraayenhof-cuvette⁵⁰ with temperature control, stirring, and light-input ports. Measurements were carried out in buffer (20 mM Tris-HCl, 10 mM NaCl, pH 8.0) at temperatures as described in the text. Where applicable, samples were illuminated with a blue LED ($\lambda_{\text{max}} = 464$ nm, full width at half-maximum (FWHM) = 25 nm) of which the intensity could be controlled. Recovery kinetics were fitted to an exponential function using Microsoft Excel 2010 and non-linear regression analysis, essentially as described in Brown (2001).⁵¹ The spectrum of YtvA in the light-induced signaling state was obtained by bleaching with high intensity white light from a SCHOTT KL 1500 LCD source, while the spectrum of YtvA in the dark state was determined after full recovery. Light intensities were measured using a LI-COR LI-250 light meter and a LI-COR Quantum Sensor.

For the measurements with varying light intensities (Fig. 3) whole spectra were monitored until equilibrium was reached. To ensure that results of different experiments and samples were comparable, each spectrum was baseline-corrected by setting the average absorption between 525 and 535 nm to zero, and subsequently normalized to the isosbestic point at 410 nm. The fraction of protein still in the dark state was then calculated by treating the spectrum as a linear combination of similarly corrected full dark and full light spectra. The R63K mutant of YtvA was treated in the same way. However, this mutant was slightly sensitive to bleaching at 37 °C and high light intensities. To correct for this, dark spectra were determined after each measurement, and the calculations of the fraction of the protein in the dark state and in the light-induced signaling state were adjusted accordingly. In addition, fresh protein samples were used whenever significant bleaching was detected. Bleaching was not an issue for the R63K mutant at 19 °C, nor for the wild type at 37 °C.

***In vivo* GSR activation assays and data analysis**

For all experiments, Tryptic Soy Broth (TSB) medium was used, supplemented with 0.5% (w/v) glucose, 5 $\mu\text{g ml}^{-1}$ chloramphenicol and 10 $\mu\text{g ml}^{-1}$ kanamycin. Cells were continuously kept at 37 °C

in a water bath. To ensure sufficient aeration, cells were always shaken at 250 rpm in an orbital shaker with no more than 10 ml of culture in a 100 ml Erlenmeyer flask.

To initiate an experiment, 10 ml of medium was inoculated and cells were allowed to grow overnight. Such cultures were diluted to an OD at 600 nm of 0.05 and allowed to grow until an OD₆₀₀ of approximately 0.6. At this point, expression of (wild-type or mutant) YtvA was induced by the addition of IPTG to a final concentration of 1 mM. Next, cells were allowed to grow until they reached an OD₆₀₀ of approximately 2.0 (late exponential growth phase), when they were again diluted to an OD₆₀₀ of 0.05. This dilution was divided over 16 flasks which were incubated until an OD₆₀₀ of approximately 0.5 was reached. A control sample was taken (time point 0), and the light was switched on. Additional samples were then taken after 120 minutes. Samples were immediately flash-frozen in liquid nitrogen and stored at -80 °C. Note that experiments were stopped before the cells reached a stationary phase to prevent activation of the GSR *via* the energy-stress branch of the upstream activation network.

Illumination was provided by blue LEDs with a λ_{max} at 464 nm. All experiments were carried out in a dark room to prevent uncontrolled illumination before time point 0. Each experiment included at least two dark controls, which were wrapped tightly in aluminum foil. Samples of dark controls and of cells prior to time point 0 were taken in complete darkness or with minimal background illumination from a red LED ($\lambda_{\text{max}} = 632$ nm), which was previously shown not to activate YtvA.^{2,22} Light intensities were measured with a LI-COR LI-250 light meter and a LI-COR Quantum Sensor.

β -galactosidase activities were measured and expressed in Miller units according to a previously described protocol.² The resulting GSR activation at varying light intensities was analyzed in Microsoft Excel 2010 using non-linear regression analysis, essentially as described in Brown (2001).⁵¹ Data were fitted to the analytically derived equation for the fraction of protein in the light-induced signaling state (S) (eqn (7) or (16)). The recovery rate (k_{re}) was left free, while all other parameters were fixed to the values specified in the text.

Light-induced branching reaction

The presence of the light-induced branching reaction was demonstrated using an Agilent 8453 UV-Vis spectrophotometer (Agilent Technologies). A quartz cuvette with a path length of 1 cm at room temperature without stirring was used. A sample of YtvA was illuminated with a blue LED ($\lambda_{\text{max}} = 464$ nm, FWHM = 25 nm) at maximum light intensity to completely convert YtvA to the light-induced signaling state. When the light source was removed YtvA slowly recovered to the dark state, which was monitored at 450 nm with a time resolution of 0.1 s. The branching reaction was immediately induced by photo-excitation with the third-harmonic of light from a Continuum Surelite I-10 YAG laser with an output intensity of 100 mJ at 355 nm and a pulse duration of 6 ns.

The quantum yield of the light-induced branching reaction was estimated from the equilibrium between dark state (D) and

light-induced signaling state (S) at saturating light intensities of a light source absorbed by both species, as explained in the Results section. Experiments were carried out in the same setup as described above for the *in vitro* photocycle measurements. A temperature of 25 °C was used to ensure that thermal recovery would be negligible. As the light source, a custom-made LED with a λ_{max} of 401 nm (FWHM of 12 nm) and a variable intensity was used. Data was processed analogous to the blue light *in vitro* experiments described above, using Matlab R2010b (MathWorks) and Microsoft Excel 2010.

Note added in preparation

While this paper was in the preparation and submission process Losi *et al.* published an intriguing paper on super-resolution microscopy using YtvA in which the existence of the branching reaction is also convincingly demonstrated.⁵² Their data confirms our observation that the quantum yield of this branching reaction is low, which further solidifies our conclusions with respect to the biological implications.

Author contributions

JBvdS and YN performed experiments; JH, JBvdS, KJH and YN developed models; JBvdS, YN and KJH designed experiments; and JBvdS wrote the paper.

Conflict of interest

The authors declare that they have no conflict of interest.

Acknowledgements

The authors would like to acknowledge the help of Jos C. Arents and Francis K. Fordjour with experiments, to thank Wolfgang Gärtner for kindly providing a strain, and to thank Chris de Koster for critical reading of the manuscript.

References

- M. A. van der Horst and K. J. Hellingwerf, *Acc. Chem. Res.*, 2004, **37**, 13–20.
- M. Avila-Perez, K. J. Hellingwerf and R. Kort, *J. Bacteriol.*, 2006, **188**, 6411–6414.
- A. Losi, E. Polverini, B. Quest and W. Gartner, *Biophys. J.*, 2002, **82**, 2627–2634.
- G. P. Pathak, A. Losi and W. Gartner, *Photochem. Photobiol.*, 2012, **88**, 107–118.
- U. Krauss, B. Q. Minh, A. Losi, W. Gartner, T. Eggert, A. von Haeseler and K. E. Jaeger, *J. Bacteriol.*, 2009, **191**, 7234–7242.
- A. Losi and W. Gartner, *Photochem. Photobiol. Sci.*, 2008, **7**, 1168–1178.
- A. Losi, *Photochem. Photobiol. Sci.*, 2004, **3**, 566–574.
- M. A. van der Horst, J. Key and K. J. Hellingwerf, *Trends Microbiol.*, 2007, **15**, 554–562.
- A. Losi, B. Quest and W. Gartner, *Photochem. Photobiol. Sci.*, 2003, **2**, 759–766.
- C. W. Price, P. Fawcett, H. Ceremonie, N. Su, C. K. Murphy and P. Youngman, *Mol. Microbiol.*, 2001, **41**, 757–774.
- J. D. Helmann, M. F. Wu, P. A. Kobel, F. J. Gamo, M. Wilson, M. M. Morshedi, M. Navre and C. Paddon, *J. Bacteriol.*, 2001, **183**, 7318–7328.
- A. Petersohn, M. Brigulla, S. Haas, J. D. Hoheisel, U. Volker and M. Hecker, *J. Bacteriol.*, 2001, **183**, 5617–5631.
- N. Suzuki, N. Takaya, T. Hoshino and A. Nakamura, *J. Gen. Appl. Microbiol.*, 2007, **53**, 81–88.
- J. B. van der Steen, M. Avila-Perez, D. Knippert, A. Vreugdenhil, P. van Alphen and K. J. Hellingwerf, *J. Bacteriol.*, 2012, **194**, 1708–1716.
- M. Hecker, J. Pane-Farre and U. Volker, *Annu. Rev. Microbiol.*, 2007, **61**, 215–236.
- C. C. Chen, R. J. Lewis, R. Harris, M. D. Yudkin and O. Delumeau, *Mol. Microbiol.*, 2003, **49**, 1657–1669.
- O. Delumeau, C. C. Chen, J. W. Murray, M. D. Yudkin and R. J. Lewis, *J. Bacteriol.*, 2006, **188**, 7885–7892.
- J. Marles-Wright and R. J. Lewis, *Commun. Integr. Biol.*, 2008, **1**, 182–184.
- S. Akbar, T. A. Gaidenko, C. M. Kang, M. O'Reilly, K. M. Devine and C. W. Price, *J. Bacteriol.*, 2001, **183**, 1329–1338.
- T. A. Gaidenko, T. J. Kim, A. L. Weigel, M. S. Brody and C. W. Price, *J. Bacteriol.*, 2006, **188**, 6387–6395.
- M. Jurk, P. Schramm and P. Schmierer, *Biochem. Biophys. Res. Commun.*, 2013, **432**, 499–503.
- M. Avila-Perez, J. B. van der Steen, R. Kort and K. J. Hellingwerf, *J. Bacteriol.*, 2010, **192**, 755–762.
- Y. Tang, Z. Cao, E. Livoti, U. Krauss, K. E. Jaeger, W. Gartner and A. Losi, *Photochem. Photobiol. Sci.*, 2010, **9**, 47–56.
- B. D. Zoltowski, B. Vaccaro and B. R. Crane, *Nat. Chem. Biol.*, 2009, **5**, 827–834.
- J. Hendriks and K. J. Hellingwerf, *J. Biol. Chem.*, 2009, **284**, 5277–5288.
- A. Miller, H. Leigeber, W. D. Hoff and K. J. Hellingwerf, *Biochim. Biophys. Acta, Bioenerg.*, 1993, **1141**, 190–196.
- J. Hendriks, I. H. van Stokkum, W. Crielaard and K. J. Hellingwerf, *FEBS Lett.*, 1999, **458**, 252–256.
- E. Ritter, M. Elgeti and F. J. Bartl, *Photochem. Photobiol.*, 2008, **84**, 911–920.
- J. L. Spudich and R. A. Bogomolni, *Nature*, 1984, **312**, 509–513.
- F. J. Bartl, E. Ritter and K. P. Hofmann, *J. Biol. Chem.*, 2001, **276**, 30161–30166.
- N. Hazemoto, N. Kamo, M. Kondo and Y. Kobatake, *Biochim. Biophys. Acta, Bioenerg.*, 1982, **682**, 67–74.
- N. C. Rockwell, Y. S. Su and J. C. Lagarias, *Annu. Rev. Plant Biol.*, 2006, **57**, 837–858.
- J. T. Kennis, I. H. van Stokkum, S. Crosson, M. Gauden, K. Moffat and R. van Grondelle, *J. Am. Chem. Soc.*, 2004, **126**, 4512–4513.
- T. E. Meyer, G. Tollin, J. H. Hazzard and M. A. Cusanovich, *Biophys. J.*, 1989, **56**, 559–564.

- 35 T. Lamparter, B. Esteban and J. Hughes, *Eur. J. Biochem.*, 2001, **268**, 4720–4730.
- 36 M. Rehorek and M. P. Heyn, *Biochemistry*, 1979, **18**, 4977–4983.
- 37 J. Marles-Wright, T. Grant, O. Delumeau, G. van Duinen, S. J. Firbank, P. J. Lewis, J. W. Murray, J. A. Newman, M. B. Quin, P. R. Race, A. Rohou, W. Tichelaar, M. van Heel and R. J. Lewis, *Science*, 2008, **322**, 92–96.
- 38 S. Kalman, M. L. Duncan, S. M. Thomas and C. W. Price, *J. Bacteriol.*, 1990, **172**, 5575–5585.
- 39 U. W. Liebal, P. K. Sappa, T. Millat, L. Steil, G. Homuth, U. Volker and O. Wolkenhauer, *Mol. BioSyst.*, 2012, **8**, 1806–1814.
- 40 R. Garcia-Contreras, P. Vos, H. V. Westerhoff and F. C. Boogerd, *FEBS J.*, 2012, **279**, 4145–4159.
- 41 K. van Eunen, J. Bouwman, P. Daran-Lapujade, J. Postmus, A. B. Canelas, F. I. Mensonides, R. Orij, I. Tuzun, J. van den Brink, G. J. Smits, W. M. van Gulik, S. Brul, J. J. Heijnen, J. H. de Winde, M. J. de Mattos, C. Kettner, J. Nielsen, H. V. Westerhoff and B. M. Bakker, *FEBS J.*, 2010, **277**, 749–760.
- 42 A. Goel, F. Santos, W. M. Vos, B. Teusink and D. Molenaar, *Appl. Environ. Microbiol.*, 2012, **78**, 134–143.
- 43 J. C. Locke, J. W. Young, M. Fontes, M. J. H. Jimenez and M. B. Elowitz, *Science*, 2011, **334**, 366–369.
- 44 O. A. Igoshin, M. S. Brody, C. W. Price and M. A. Savageau, *J. Mol. Biol.*, 2007, **369**, 1333–1352.
- 45 D. Bray, *J. Mol. Biol.*, 2013, **425**, 1410–1414.
- 46 M. Kollmann and V. Sourjik, *Curr. Biol.*, 2007, **17**, R132–R134.
- 47 C. A. Velds, P. C. T. van der Hoeven, J. M. Koopstra, W. R. Raaff and W. H. Slob, *Zonnestraling in Nederland*, Koninklijk Nederlands Meteorologisch Instituut/Thieme, Baarn, The Netherlands, 1992.
- 48 C. A. Gueymard, *Sol. Energy*, 2001, **71**, 325–346.
- 49 S. A. Boylan, A. Rutherford, S. M. Thomas and C. W. Price, *J. Bacteriol.*, 1992, **174**, 3695–3706.
- 50 R. Kraayenhof, J. J. Schuurmans, L. J. Valkier, J. P. Veen, D. Van Marum and C. G. Jasper, *Anal. Biochem.*, 1982, **127**, 93–99.
- 51 A. M. Brown, *Comput. Methods Programs Biomed.*, 2001, **65**, 191–200.
- 52 A. Losi, W. Gartner, S. Raffelberg, F. Cella Zanacchi, P. Bianchini, A. Diaspro, C. Mandalari, S. Abbruzzetti and C. Viappiani, *Photochem. Photobiol. Sci.*, 2013, **12**, 231–235.
- 53 M. J. Casadaban and S. N. Cohen, *J. Mol. Biol.*, 1980, **138**, 179–207.
- 54 P. Stragier, C. Bonamy and C. Karmazyn-Campelli, *Cell*, 1988, **52**, 697–704.
- 55 M. Avila-Perez, J. Vreede, Y. Tang, O. Bende, A. Losi, W. Gartner and K. Hellingwerf, *J. Biol. Chem.*, 2009, **284**, 24958–24964.